Measurement of the Stark shift within the $6P_{1/2}$-$7S_{1/2}$ 378-nm transition in atomic thallium

S. C. Doret,* P. D. Friedberg,† A. J. Speck,* D. S. Richardson,‡ and P. K. Majumder§
Physics Department, Williams College, Williamstown, Massachusetts 01267
(Received 17 July 2002; published 19 November 2002)

Using a thallium atomic beam apparatus and a stabilized, frequency-doubled diode laser system, we have measured the scalar Stark shift in the $6P_{1/2}$-$7S_{1/2}$ transition of thallium. We determine the Stark shift to be $\Delta\nu_S = -103.23(39)$ kHz/(kV/cm)^2, providing more than an order of magnitude improvement in precision over earlier measurements of this quantity. This measurement serves as a stringent test of recently published thallium parity nonconservation calculations.

DOI: 10.1103/PhysRevA.66.052504 PACS number(s): 32.10.Dk, 32.60.+i, 32.70.Jz, 32.30.Jc

I. INTRODUCTION

In recent years, atomic parity nonconservation (PNC) experiments [1,2] have achieved precision sufficient to provide sensitive tests of the standard electroweak model. For the case of cesium, there has been a substantial amount of recent theoretical work aimed at pushing the necessary wave-function calculations in this element beyond the 1% level of precision [3]. The current level of activity reflects the importance of this standard model test, but also highlights the challenges associated with pushing such calculations to the sub-1% level. In thallium, a new round of wave-function calculations were also recently completed [4]. This new result now requires a variety of independent thallium atomic structure measurements of high precision to provide cross-checks on accuracy, and to guide the further development of the theory. Ultimately, there would be no more satisfying test of both PNC experiment and atomic theory than to develop consistent standard model tests of comparable overall precision in more than one atomic system.

Recently in our group, we completed a precise measurement of the electric quadrupole transition amplitude [5] as well as hyperfine splitting and isotope shift measurements [6] within the two lowest-lying transitions in thallium. Both of these experiments made use of thallium atoms in heated vapor cells, and the latter measurement required the development of a frequency-doubled diode laser optical system operating at 378 nm.

Here we report on the results of a high-precision measurement of the Stark shift within the same 378-nm $6P_{1/2}$-$7S_{1/2}$ $E1$ transition in thallium. For this work, we have developed a collimated atomic beam source, and performed transverse transmission spectroscopy in the presence of a large, precisely calibrated electric field. The precision of our Stark shift result represents an improvement by a factor of 15 over earlier results [7,8], and now substantially exceeds the precision quoted for the new thallium PNC calculation. We thus provide a challenging test of thallium wave-function calculations. Inasmuch as our result tests the accuracy of the long-range behavior of the wave functions, it is quite complementary to our recent hyperfine splitting and isotope shift measurements, which focus on the behavior of the wave functions near the nucleus. Two quite different measurement schemes were used to complete this experiment, each of which provided results of high precision. Their sensitivity to a variety of potential systematic errors was quite complementary, making the consistency of the results particularly notable.

II. ATOMIC STRUCTURE DETAILS

There are two naturally occurring isotopes of thallium, ^{205}Tl (70.5%) and ^{203}Tl (29.5%), each of which has nuclear spin $I=1/2$, so that both the $6P_{1/2}$ and $7S_{1/2}$ states contain $F=0$ and $F=1$ hyperfine levels. The respective 21- and 12-GHz hyperfine splittings (HFS) of the ground and excited states, and the relatively large 1.7-GHz transition isotope shift (IS) [6], yield an entirely resolved spectrum in our atomic beam apparatus. Because we study a $J=1/2\rightarrow J=1/2$ transition, the Stark shift of each level, ΔW, has only a scalar component, producing a common shift of all sublevels within a given state, and yielding an experimental result that is independent of relative laser and static electric-field polarization. Expressing the Stark shift of a given level as $\Delta W = -\frac{1}{2}\alpha_0 E^2$, where α_0 is the scalar polarizability, the observed frequency shift of the 378-nm line can then be expressed as $\Delta\nu_S = -(1/2h)[\alpha_0(7S_{1/2}) - \alpha_0(6P_{1/2})]E^2$. The polarizability of each level is calculable from second-order perturbation theory. For example, in the one-electron central field approximation, it is straightforward to show that [9,10]

$$\alpha_0(7S_{1/2}) = \frac{2e^2}{9}[\xi(7s_{1/2},p_{1/2}) + 2\xi(7s_{1/2},p_{3/2})],$$

$$\alpha_0(6P_{1/2}) = \frac{2e^2}{9}[\xi(6p_{1/2},s_{1/2}) + 2\xi(6p_{1/2},d_{3/2})],$$

where the ξ's represent particular infinite sums of radial integrals. For example,

*Present address: Department of Physics, Harvard University, Cambridge, MA 02138.
†Present address: Department of Electrical Engineering and Computer Sciences, University of California, Berkeley, CA 94720.
‡Present address: Department of Chemistry and Physics, NW Missouri State University, Maryville, MO 64468.
§Electronic address: pmajumde@williams.edu

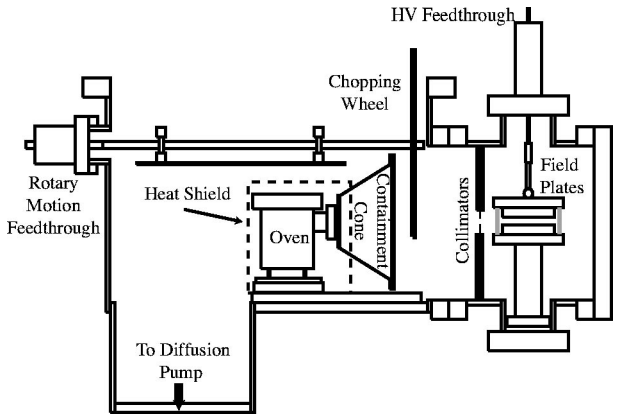

FIG. 1. A sketch of the overall atomic beam apparatus. The distance from source to interaction region is 30 cm.

$$\xi(6p_{1/2},l_J)=\sum_n \frac{\left(\int_0^\infty R(6P_{1/2})rR(nl_J)d^3r\right)^2}{(E_{nl_J}-E_{6p_{1/2}})}.$$

Furthermore, due to the size of the HFS and IS compared to the optical transition frequencies ($\delta\nu_{HFS}/\delta\nu_{opt}$ and $\delta\nu_{IS}/\delta\nu_{opt}$ are of order 10^{-5} and 10^{-6}, respectively) we expect no measurable difference in Stark-shift value among the six isotopic and hyperfine component lines, given our level of experimental precision. Small tensor components to the Stark shift of individual sublevels induced by higher-order hyperfine interaction effects are similarly of negligible magnitude in our experiment [11]. The work described here has therefore centered exclusively on the strongest $F=1 \rightarrow F=1$ transition of ^{205}Tl.

In this experiment, we detect the UV laser light transmitted through the atomic beam, which exhibits a roughly 40% reduction on resonance of this particular hyperfine transition. As we cannot approximate the atomic sample as ''optically thin,'' we analyze our transmission spectra according to $T(\nu)=\exp[-\beta\mathcal{V}(\gamma,\Gamma;\nu)]$. Anticipating that we will normalize the signal to the ''no atoms'' condition, we need not include any additional overall normalization factor. Here $\beta \approx 0.5$ is the optical depth and $\mathcal{V}$ is the normalized Voigt profile which characterizes our absorption line shape. The residual Doppler (full) width Γ is roughly 100 MHz, while the Lorentzian component of the profile, γ, contributes roughly 20 MHz due to the $7S_{1/2}$-state natural lifetime.

III. APPARATUS AND EXPERIMENTAL DETAILS

A. Atomic beam system

Referring to Fig. 1, we produce our thallium thermal atomic beam by heating roughly 300 g of thallium in a heat-shielded stainless-steel oven to a temperature of 750–800 °C via 0.6 kW of ac power supplied to a heating element (Philips ''Thermocoax'') wrapped around the oven. Atoms exit the oven from a nozzle of overall width 2 cm. The nozzle consists of 32 parallel vertical ''tunnels'' of width 0.25 mm, height and depth 0.5 cm. This design allows for a favorable combination of total throughput and beam collimation. To avoid clogging, the nozzle assembly is heated by a second heating element, and it maintains a temperature roughly 50 °C higher than the oven body. Nested cones are positioned immediately downstream of the oven nozzle. These cones keep uncollimated thallium away from the path of the beam, and allow for straightforward recycling of solidified thallium metal back into the oven. A knife-edged aperture centered on the downstream plate of the cone assembly, whose dimension matches the 2 cm$\times$0.5 cm nozzle extent, aids in beam collimation. In this way, the vast majority of the thallium metal exiting the oven can be recovered with minimal contamination of the rest of the source chamber. The source chamber itself is a 45-cm-diameter, 30-cm-high cylindrical stainless-steel structure, with vacuum ports allowing for electrical and thermocouple feedthroughs, vacuum gauges, and a ferrofluidic rotary motion feedthrough. A liquid-N_2-trapped diffusion pump (Varian M-6) maintains a chamber pressure of roughly 5×10^{-7} torr when the oven is hot.

In a 20-cm-diameter, 20-cm-long extension tube protruding from the source chamber, we position two pairs of razor blades mounted on translation feedthroughs. Located 20-cm downstream of the oven nozzle, these allow final collimation and definition of both the horizontal and vertical extents of the atomic beam. We typically set the vertical blades 2-mm apart, and the horizontal pair 1.5-cm apart. A set of three orthogonal magnetic-field coils limit the residual magnetic field in our interaction region to $\leqslant$10 mG in all directions.

B. High-voltage system and electric-field calibration

Our interaction region, located 30 cm downstream of the oven, consists of a pair of polished stainless-steel plates of diameter 8 cm separated by four ceramic spacers. The entire assembly is mounted on a 5-cm-diameter ceramic post attached to a vacuum flange beneath the interaction region with adjustable screws. Metric gauge blocks are used during the assembly of the field plates and we determine the plate separation to be 1.0002(2) cm. Repeated measurements of this separation at later times revealed no measurable change. The modest temperature increase, characteristic of the downstream interaction region during beam operation, causes negligible change in plate separation, especially given that expansion of the ceramic posts and steel plates tend to oppose one another. The UV laser beam intersects the 1.5-cm-wide atomic beam at the center of the plate assembly. Independently, we have performed simulations to insure that, given our interaction region geometry, any nonidealities due to the finite size of the plates would affect our electric field calibration only at the level of 1 part in 10^5 or below.

A high-voltage power supply (Spellman CZE2000) allows the application of up to 30 kV to the plates. Our data-acquisition system allows computer control of both polarity and magnitude of this voltage. In series with the high-voltage output and the field plates, we place both a chain of resistors of total resistance 100 MΩ (for current limiting and power supply protection), as well as a 1 MΩ resistor between the ground plate and the power supply return (for leakage current monitoring). When free of any thallium deposits, the

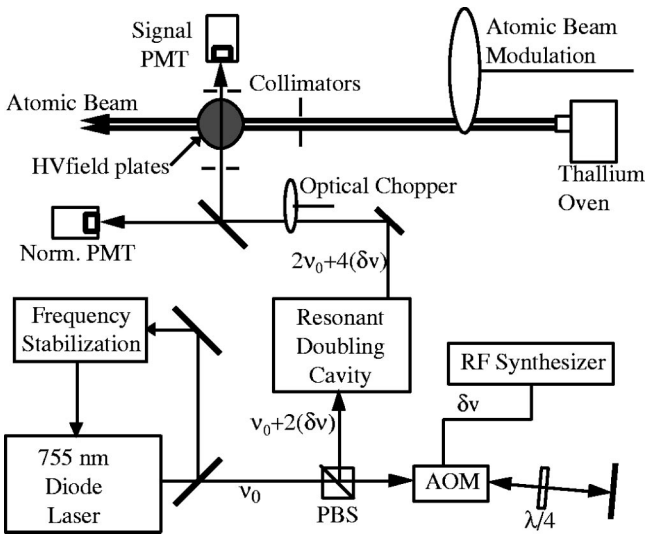

FIG. 2. Schematic diagram of the optical system and interaction region.

field plate system exhibited leakage currents of order 1 nA even at the highest voltages. After several weeks of running, this number increased to 100 nA, though it remained substantially less for lower voltages. In parallel with the power supply, we installed a commerical voltage divider (Ross Engineering, Inc.). This device has a quoted precision of 0.01%, total resistance of 180 MΩ, and is customized so that it is impedance matched to the particular voltmeter we use (Keithley model 197*A*, 0.011% absolute voltage measurement accuracy). The data-acquisition program reads the output of the Keithley voltmeter, which, to the quoted precision of the instruments, is exactly 1/1000 of the actual high-voltage applied. Errors due to leakage-current-induced voltage drops are negligible at this level.

C. Optical system

The optical system used to generate the 378-nm light required to excite the transition achieves two primary goals—frequency stabilization of our laser source and precise frequency tunability. Referring to Fig. 2, we begin with an external-cavity ''Littrow'' configuration diode laser system producing roughly 15 mW of light at 755 nm (Sacher Lasertechnik TEC 100). The laser is stabilized based on a scheme described in Ref. [12]. We send two lasers into a temperature stabilized Fabry-Perot cavity (Burleigh RC-11)—our diode laser and a commericially stabilized helium-neon laser (Melles Griot 05 STP 901). A computer is responsible for scanning the length of the cavity and collecting Fabry-Perot transmission spectra of the two lasers. The goal is to fix the location of a particular diode laser transmission peak between consecutive He-Ne peaks, thus transferring the He-Ne laser stability to the diode laser. After locating transmission peak positions, the quantity ρ, defined as the fractional position of the diode peak with respect to the He-Ne peaks is computed $(0<\rho<1)$. A correction signal, sent to the piezoelectric transducer (PZT) in the diode laser external cavity, is generated by comparing ρ to a setpoint and utilizing a software *P-I-D* feedback loop. We are thus able to steer the diode laser frequency by updating the PZT voltage at a rate of roughly 30 Hz (limited by the speed of the computer). This is sufficient to reduce long-term drifts to the 0.8 MHz/h specifications of the stabilized He-Ne laser. We continue to observe residual short-term diode laser frequency jitter of roughly 1.5 MHz (rms).

Frequency tuning of the frequency-stabilized light is achieved via a double pass through an acousto-optic modulator (AOM) (Isomet 1206*C*), providing rapid, computer-controlled tuning of synthesizer precision. Following the double pass through the AOM, we generate the final 378-nm light by frequency doubling in an external resonant cavity (Laser Analytical Systems Wavetrain-CW). This bowtie-configuration ring cavity contains a lithium triborate crystal at the focal point. Though the efficiency limitations of our AOM limit us to a 25-MHz tuning range in order to achieve reasonable UV output, we benefit from the fourfold multiplication afforded by AOM double passing *and* frequency doubling. Thus, we eventually obtain a minimum of 300 nW of UV light tunable over a 100-MHz range, which is sufficient to calibrate Stark shifts at our maximum electric fields, as described below. This light is then focused onto the atomic beam through 0.5-mm collimators located on either side of the interaction region and separated by 50 cm. This tight geometric collimation allows us to place limits on potential systematic effects of residual beam steering, as discussed in Sec. V below.

D. Data collection and signal processing

Data collection occurs via two identical photomultiplier tubes (Hamamatsu *R*1527) and associated preamplifiers—one to make transmission measurements and one for normalization purposes to correct for laser intensity fluctuations. The data are normalized for a second time by computing the ratio of transmission with the atomic beam to that measured with the atoms blocked via a slow (1-Hz) modulation driven by a stepping motor. This ''twice-normalized'' signal (referred to as ''*T*'' below) thus varies between 0 (complete absorption of laser light) and 1 (atoms blocked), and is largely immune to slow drifts in the system, atomic beam density fluctuations, etc. Signal to noise is further improved via a more rapid ($\approx$1500-Hz) laser beam modulation and subsequent detection of the two photomultiplier tube (PMT) signals in a pair of lock-in amplifiers (Stanford Research Systems Model 8100). Finally, the effects of any linear drifts in the system are substantially reduced by taking all measurements as a difference between electric-field-on and electric-field-off configurations, collecting these pairs of points in both possible orders, and averaging the results.

E. Overview of experimental method

During the course of this work, as an alternative to the more straightforward technique of obtaining spectral scans for a variety of electrical field values, we developed a quite different measurement procedure for obtaining precise Stark shift results. This technique, which we refer to as the ''transmission change'' method, can determine the Stark shift rapidly and precisely without the need for complete scans of the

resonance line shape. Essentially, we lock the laser near the steep inflection point on the side of the atomic resonance. Then, by changing the AOM frequency by a known amount and simultaneously applying an appropriate range of known electric fields, one interpolates the exact field required to offset a given frequency shift.

In further detail, one first chooses a laser lockpoint that corresponds to a point roughly 60% of the way down to the bottom of the transmission dip for the particular hyperfine resonance under study. This insured that we were located near the inflection point of the curve, and also minimized potential systematic errors due to curve nonlinearity, as described in the following section. We sample both the laser transmission and normalization signals from the lock-in amplifier outputs while the stepper motor controlling the atomic beam chopping wheel blocked and unblocked the atomic beam at roughly 1 Hz (in an on-off-off-on format to minimize drift-induced systematics). The data-acquisition program then computed the value of the normalized laser transmission signal T_0, as defined above. These data, taken with no electric field present, correspond to experimental configuration ''*A*.'' At this point, we simultaneously apply a known electric field (in the range of 15–30 kV/cm), and, based on an approximate value for the Stark-shift constant, apply an appropriate (downward) shift to the AOM frequency (i.e., one-quarter of the desired UV frequency shift). The resulting value of the new transmission signal T was within a few percent of T_0. This second experimental configuration ''*B*'' was then repeated, after which we returned to configuration *A*. Acquiring consecutive pairs of transmission change data in this *ABBA* format allowed us to monitor and reduce possible systematics due to slow drifts in the system. The dwell time in each configuration was typically 10 sec, the first half of which was dead time, allowing for voltage switching transients to decay away.

The entire procedure was then repeated with the only change being a slightly different choice of electric field. All together, five electric-field values were used. The order of field values was selected randomly, and, overall, represented a fractional change in the value of E^2 of $\pm 5-10\,\%$. By fitting a linear function to a plot of E^2 vs $\Delta T \equiv T - T_0$, we could determine the particular value of the electric field (squared), which exactly compensated for the UV frequency shift chosen for that run. Both at the beginning and the end of a run, to insure that there has been no overall drift in optical depth, which might produce a systematic error, we shift the electric field such that the current laser frequency corresponds to the exact resonance line center of the Stark-shifted curve and sample the value of T here. This entire procedure takes roughly 20 min. At this point, we manually change the laser lockpoint to the symmetric location on the other side of the atomic resonance. Many potential systematic errors tend to cancel when results from low- and high-frequency side lockpoints are averaged. Agreement among results for the two configurations (as we have observed) is good evidence for the lack of such systematic errors.

IV. DATA AND ANALYSIS

Figure 3 shows the data and linear fits to one particular pair of transmission change data runs. The y intercepts extracted from the fits agree within their respective uncertainties, and the overall precision of this run is better than 2%. The value of the Stark-shift constant, $\Delta\nu_S$, is then recorded as the ratio of the UV frequency shift for a given data run divided by the fitted y intercept. About 100 individual runs were accumulated over a period of 2 months, during which we varied as many experimental operating conditions as possible. Data were taken over a wide range of nominal electric-field values, for several values of atomic beam collimation widths, and, as discussed, for lockpoints on both sides of the atomic resonance. Most important, we made an effort to choose laser lockpoints at various points along the resonance curve, including points far from the nominal point of inflection to explore potential systematic errors associated with the nonlinearity of the curve. The 70 runs used in our final analysis are represented in Fig. 4 in both scatter plot and histogram form, where the individual error bars shown simply reflect the uncertainty in y-intercept determination of the linear fit. The reduced χ^2 of this distribution is 1.15, and the histogram of the results is modeled very well by a Gaussian. This analysis of our transmission change data yields a Stark-shift value of $\Delta\nu_S = -103.39 \pm 0.20$ kHz/(kV/cm)^2, where the statistical error is taken from the standard error associated with the best fit Gaussian indicated in Fig. 4(b).

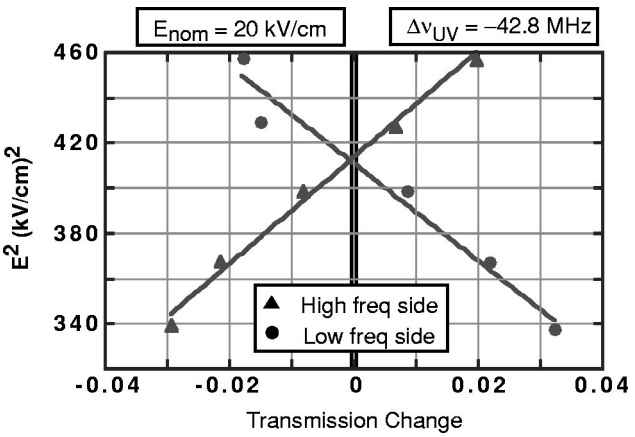

FIG. 3. A typical data run using the transmission change method. Data are shown for both low- and high-side laser lock. The roughly $\pm 10\%$ range in E^2 results in a few percent change in transmission between configurations *A* and *B* (see text). For this run, the UV frequency shift was -42.8 MHz throughout. The common y intercept of ≈ 413 (kV/cm)^2 yields a Stark-shift constant of $\Delta\nu_S = -103.6(1.5)$ kHz/(kV/cm)^2 for these data.

V. EXPLORATION OF SYSTEMATIC ERRORS

As introduced above, this experimental technique relies upon fitting a line to a small region of the absorption line shape to interpolate what electric-field strength is required to exactly offset the transmission change induced by a particular shift in laser frequency. Because the line shape is inherently nonlinear, we explored in great detail the potential systematic errors associated with this linear approximation. To guide our choice of experimental parameters (laser lockpoint, range of variation of E^2 values, and so on), computer simulations of the experimental procedure were performed

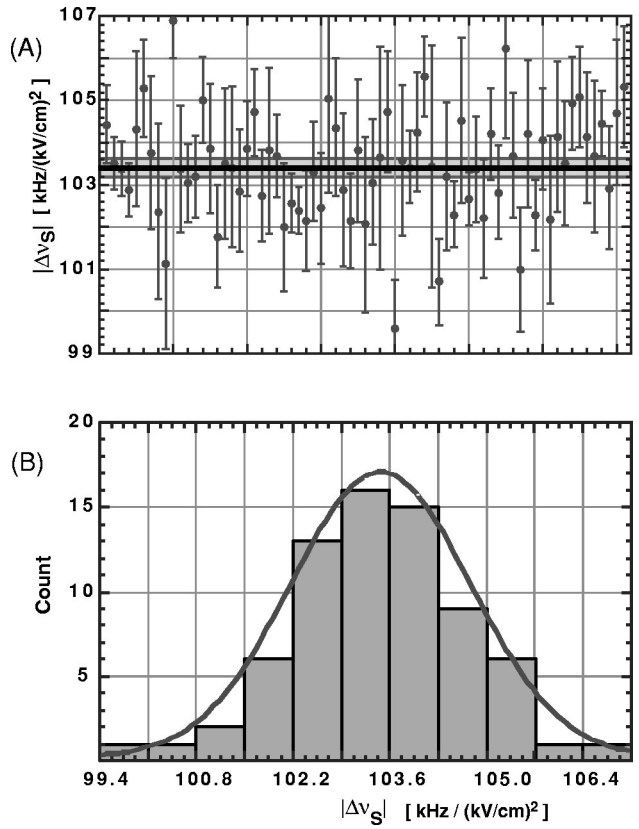

FIG. 4. Scatter plot (a) and histogram (b) of all transmission change data. The mean and standard error are shown for the scatter plot. The standard error associated with the best-fit Gaussian to the histogram data corresponds to 0.20 kHz/$(\mathrm{kV/cm})^2$.

using Voigt profiles similar to those measured in our experiment. These simulations indicated that, for our experimental conditions, the minimum systematic error due to line shape nonlinearity would result from locking the laser to the inflection point, roughly 60% of the way down the transmission dip towards its peak in our case. Furthermore, it was confirmed that the sign of the error introduced by the linear fit changes sign for data taken on the high- vs low-frequency side of the line shape, such that data taken with the laser locked to a symmetric pair of locations with identical (normalized) transmission could be averaged to obtain the true Stark shift. Such averaging would also address any possible electric-field-induced changes in linewidth.

Ultimately, each data run explicitly included data taken on both the low- and high-frequency sides of the atomic line. For most runs the laser was locked near the inflection point of the curve. However, to explore potential systematic effects, data were collected at a wide variety of laser lockpoints ranging from 0.2 (in the wings of the absorption profile) to 0.9 (near the peak). A correlation plot of *all* measured values of $\Delta\nu_S$ against lockpoint did show a systematic effect (resolved at the level of about 2σ) in spite of the fact that data were collected on both sides of the atomic absorption line. However, when only data collected in a more restricted region near the inflection point were included in the analysis, no resolved systematic effect remained, as shown in Fig. 5. To further confirm that no resolved systematic effect remained, comparisons were made between values from linear fits to all of the data to fits based on only three inner data points of the five collected in each run with no resolved disagreement. Given that we see a resolved systematic nonlinearity effect for lockpoints far from the inflection point, we ultimately included a systematic error contribution to account for the range of lockpoints that were actually represented in our final dataset.

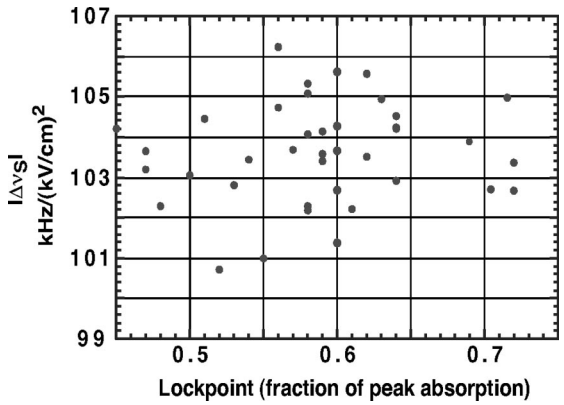

FIG. 5. An example of a correlation search. Here Stark-shift results are plotted vs laser lockpoint (as measured by location along the transmission dip, see text). The slope of the best-fit line to these data is unresolved (2.1 ± 3.1).

In addition to this correlation with laser lockpoint, the data were also examined for correlations with electric-field strength, atomic beam collimation width (thus optical depth), and, explicitly, for data taken on the low- vs high-frequency side of the profile, all of which were unresolved.

An important concern in our experiment was the small, residual beam steering that resulted from tuning the AOM, even after double passing. To explore potential errors from small Doppler shift changes correlated with AOM frequency changes, we examined the transverse intensity distribution of the laser beam as it enters the transmission PMT at two extreme values of the AOM frequency tuning range. Considering only our geometric collimation arrangement, a 0.8-MHz change in Doppler shift would be possible as a result of beam steering; yet analysis of the intensity distributions observed at the two AOM frequencies allowed us to place an upper limit of 0.05 MHz on such an effect. We note, finally, that experimental complications associated with optical saturation or optical pumping effects were not of concern to us, given the extremely low UV laser power used throughout this work. Table I identifies all significant contributors to the overall systematic error in the transmission change data analysis.

During the course of data collection, two different oven temperatures were used, separated by approximately 25 °C, giving two different clusters of data points when results were plotted against temperature. These two subsets of the data therefore reflected different atomic beam density and measured optical depth. A marginally resolved (1.5σ) difference in the averages of the data clusters was seen. To address this, we have conservatively included an associated systematic error contribution in our final error budget (see Table I). However, as discussed next, an alternative measurement method

TABLE I. Summary of contributions to the overall error in transmission change Stark-shift data (see text).

Source of error	$[\mathrm{kHz/(kV/cm)^2}]$
Statistical error	0.20
Systematic error sources	
Lockpoint (curve nonlinearity)	0.30
Oven temperature and beam density	0.26
Residual Doppler shift	0.16
E^2 step size	0.04
E-field calibration	0.01
Hi/Lo side lock	0.01
Combined total error	0.47

displayed no such systematic difference when analogous datasets were analyzed in this particular fashion.

Frequency-scan results

As a general and powerful test of potential systematic effects, then, a second measurement technique was utilized to collect additional Stark-shift data. This method was more straightforward, involving scans of the laser across the entire ^{205}Tl ($F=1\rightarrow F=1$) hyperfine resonance line shape at a variety of known electric fields. These scans were then fit to Voigt profiles to determine their centers, and values for the Stark shift extracted. The frequency scale was calibrated by using a 0.1-ppm wavemeter (Burleigh WA-1500) to calibrate the free spectral range (FSR) of the Fabry-Perot cavity which we use for frequency stabilization. In this way, we could translate the laser lockpoint ρ, defined earlier, into relative frequency, since it can be shown that $d\nu/d\rho = (\lambda_{He\text{-}Ne}/\lambda_{diode})\mathrm{FSR}$. Our calibration accuracy was 1 part in 10^4. A representative pair of scans and corresponding fits are shown in Fig. 6.

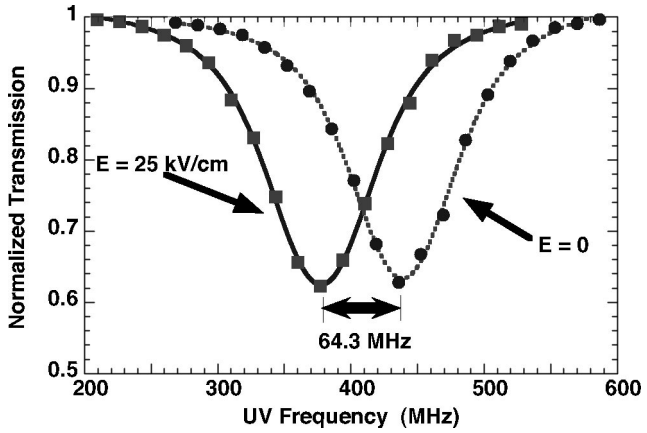

FIG. 6. Frequency scans of the ^{205}Tl ($F=1\rightarrow F=1$) hyperfine transition at zero field and with a 25 kV/cm electric field. Data points and Voigt profile fits (lines) are shown. Each data point corresponded to a particular value of ρ, the laser stabilization lock point, which was then translated into relative frequency as described in the text.

It is reasonable to consider whether nonlinearity in the PZT's used to scan the laser stabilization cavity limits our calibration accuracy. The quoted nonlinearity of the piezostacks in the scanning Burleigh RC-11 cavity used for laser stabilization is $<1\%$ over a substantial portion of their 1000-V range. Given that the peaks of our various Stark-shifted resonance curves correspond to only about 10-V changes in PZT voltage, we do not expect such residual nonlinearities to affect our quoted calibration precision in a significant way. One method of data analysis for the frequency-scan data involved plotting the resonance line centers as a function of electric field squared. Clearly, we would expect a systematic error of the type discussed here to yield a resolved nonlinearity in such a plot. We observe no such systematic deviation from linearity, even when all of our frequency-scan data are ''binned'' together into a single plot.

This method provides an appealing alternative technique as it does not involve shifting the AOM frequency, alleviating concerns of residual laser beam steering and associated Doppler shifts. As well, we do not rely on linear approximations to a nonlinear curve, so that two principal systematic concerns associated with the transmission change method described above are not applicable. On the other hand, this technique is substantially slower than the transmission change method since it requires collection of ~ 20 data points per scan, with each point requiring relocking of the laser to a new frequency. It is thus more susceptible to slow drifts in various experimental systems. These could be identified by taking a series of scans at increasing values of the electric field, and subsequently at decreasing values. A total of 40 individual Stark-shift measurements of this variety were made, yielding a result of $\Delta\nu_S = -103.02 \pm 0.42 \pm 0.46$ kHz/(kV/cm)^2, where the first error is statistical and the second is a combined systematic error (largely dominated by small residual drifts). Of particular note, when the frequency-scan results were analyzed with respect to oven temperature (as discussed above), absolutely no correlation was seen. The final result based on this frequency-scan method is in excellent agreement with that from the transmission change method, giving a convincing evidence for the lack of additional hidden systematics.

VI. FINAL RESULTS AND FUTURE WORK

We take our final value for the Stark-shift constant $\Delta\nu_S$ from the weighted average of the results from our two measurement techniques. After combining statistical and systematic error contributions, we arrive at $\Delta\nu_S = -103.23(39)$ kHz/(kV/cm)^2, where the final 0.4% error bar represents a one standard deviation uncertainty. In terms of the scalar polarizabilities, we can express our result as $[\alpha_0(7S_{1/2}) - \alpha_0(6P_{1/2})] = 122.96(47) \times 10^{-24}$ cm^3. Figure 7 shows our new measurement along with two existing measurements of this quantity. Our value differs from the result in Ref. [7] by roughly 1.5 (combined) standard deviations, while it is in good agreement with an earlier, less precise value [8]. The factor of 15 improvement in precision over the work in Ref. [7] is particularly significant in light of new calculations of PNC in thallium [4], whose estimated accu-

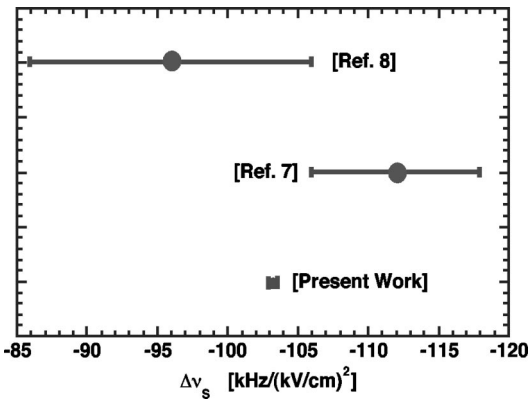

FIG. 7. A comparison of the present Stark-shift result with two older measurements.

racy is 2.5%. Any further improvements in theoretical precision will require as tests a variety of independent atomic structure measurements such as that reported here.

Of relevance to this, we are now pursuing a new atomic beam based measurement within the thallium 1283-nm $6P_{1/2}$-$6P_{3/2}$ $M1/E2$ transition. We are implementing an FM spectroscopy technique to improve the signal-to-noise ratio of our measurement of this very weak transition in the atomic beam environment. Both the Stark shift and the Stark-induced amplitude will be measured in the same transition in which PNC was measured [2]. As the $M1$ transition amplitude can be calculated precisely without the need for detailed wave-function information [4], it makes an ideal tool for number density normalization. Therefore, measuring the fractional increase in absorption upon application of a known electric field will produce a clean test of thallium atomic theory. By acquiring data for a variety of relative laser and static electric-field polarizations and by probing individual resolved hyperfine transitions, we will extract the vector and tensor components of the Stark-induced amplitude, as well as the scalar and tensor polarizability components of the Stark shift within this transition. In the course of this work, it will also be possible to make a precise, direct measurement of the small ^{205}Tl-^{203}Tl isotope shift within this transition.

ACKNOWLEDGMENTS

We would like to thank Julie Rapoport, Peter Nicholas, and Rob Lyman for help at an early stage in design and construction of the atomic beam apparatus. We gratefully acknowledge the support of the National Science Foundation RUI program (Grant No. 9721403) and the NIST Precision Measurement Grants Program (Grant No. 60NANB9D0074). We are grateful to D. Budker at U.C. Berkeley for supplying us with the oven nozzle, identical in design to that used in their atomic beam work.

[1] C.S. Wood, S.C. Bennett, D. Cho, B.P. Masterson, J.L. Roberts, C.E. Tanner, and C.E. Wieman, Science **275**, 1759 (1997).
[2] P.A. Vetter, D.M. Meekhof, P.K. Majumder, S.K. Lamoreaux, and E.N. Fortson, Phys. Rev. Lett. **74**, 2658 (1995).
[3] V.A. Dzuba *et al.*, Phys. Rev. A **63**, 044103 (2001); M.G. Kozlov *et al.*, Phys. Rev. Lett. **86**, 3260 (2001); A. Derevianko, Phys. Rev. A **65**, 012106 (2001).
[4] M.G. Kozlov, S.G. Porsev, and W.R. Johnson, Phys. Rev. A **64**, 052107 (2001).
[5] P.K. Majumder and Leo L. Tsai, Phys. Rev. A **60**, 267 (1999).
[6] D.S. Richardson, R.N. Lyman, and P.K. Majumder, Phys. Rev. A **62**, 012510 (2000).
[7] D. DeMille, D. Budker, and E.D. Commins, Phys. Rev. A **50**, 4657 (1994).
[8] T.R. Fowler and J. Yellin, Phys. Rev. A **1**, 1006 (1970).
[9] L.R. Hunter *et al.*, Phys. Rev. A **37**, 3283 (1988).
[10] A. Khadjavi, A. Lurio, and W. Happer, Phys. Rev. **167**, 128 (1968).
[11] Harvey Gould, Phys. Rev. A **14**, 922 (1976).
[12] W.Z. Zhao *et al.*, Rev. Sci. Instrum. **69**, 3737 (1998).